Journal of Sound and Vibration 329 (2010) 289–301

Contents lists available at ScienceDirect

Journal of Sound and Vibration

journal homepage: www.elsevier.com/locate/jsvi

Experimental and numerical study of a vibro-impact phenomenon in a gearshift cable

N. Leib [a,b,*], S. Nacivet [b], F. Thouverez [a]

[a] Ecole Centrale de Lyon, Laboratoire de Tribologie et Dynamique des Systèmes, UMR CNRS 5513, Equipe Dynamique des Systèmes et des Structures, 36 avenue Guy de Collongue, 69134 Ecully Cedex, France
[b] PSA Peugeot Citroën, 18 Rue des Fauvelles, 92250 La Garenne Colombes, France

ARTICLE INFO

Article history:
Received 30 June 2008
Received in revised form
8 September 2009
Accepted 16 September 2009
Handling Editor: M.P. Cartmell
Available online 12 October 2009

ABSTRACT

This paper presents a study of the nonlinear dynamic behavior of a gearshift cable and more specifically of the associated tizzing phenomenon. A gearshift cable is composed of an inner wire that can slide freely in an outer composite housing. When undergoing harmonic excitation, the inner wire interacts with the housing. Hammer and swept sine shaker tests are first used to estimate the characteristics of the two main components. It is shown that the behavior of the outer housing is nonlinear and depends on the amplitude of the excitation. The assembled gearshift cable is then set up on the shaker and the nonlinear vibro-impacting phenomenon is studied. Finally a finite element model, based on the Euler–Bernoulli beams and the Rayleigh damping coefficients, proves to offer good correlation with the measured data for different excitation frequencies. A period doubling bifurcation is observed both experimentally and numerically.

1. Introduction

Recently, vibration and acoustics have been growing concerns for car manufacturers. Most of their efforts have been concentrated on controlling the motor's vibrations with shock absorbers and different foams to limit propagation of noise and vibration to the passenger's compartment. As the biggest source of vibration is isolated, secondary vibrations and noises start to appear, such as the ones caused by the gearshift cables of either an automatic or manual transmission. Fig. 1 illustrates the global configuration of the manual gearshift under a car hood. It is composed of two cables: one that ensures gear selection and the other that engages the gear. Each cable is then itself composed of two separate pieces as shown in Fig. 2: a flexible inner wire and a protective housing. The inner wire is attached to the shift lever in the passenger's compartment at one end and to the gearbox actuator at the other end. To ensure effort transmission, the inner wire is free to slide in its housing, itself attached to the shift box at one end and to the gearbox at the other end. Since both components are fixed to the gearbox, the whole system is subject to the motor's vibrations which cause a repeated vibro-impact phenomenon where the inner wire interacts with the housing. We will refer to this phenomenon as cable "tizzing". The multiple impacts create annoying noises and vibrations that are transmitted to the shift box and into the passenger's compartment.

* Corresponding author at: Ecole Centrale de Lyon, Laboratoire de Tribologie et Dynamique des Systèmes, UMR CNRS 5513, Equipe Dynamique des Systèmes et des Structures, 36 avenue Guy de Collongue, 69134 Ecully Cedex, France . Tel.: +33156478924; fax: +33156472112.
E-mail addresses: nicholas.leib@gmail.com, nichleib@hotmail.com (N. Leib), samuel.nacivet@mpsa.com (S. Nacivet), fabrice.thouverez@ec-lyon.fr (F. Thouverez).

0022-460X/$ - see front matter © 2009 Elsevier Ltd. All rights reserved.
doi:10.1016/j.jsv.2009.09.020

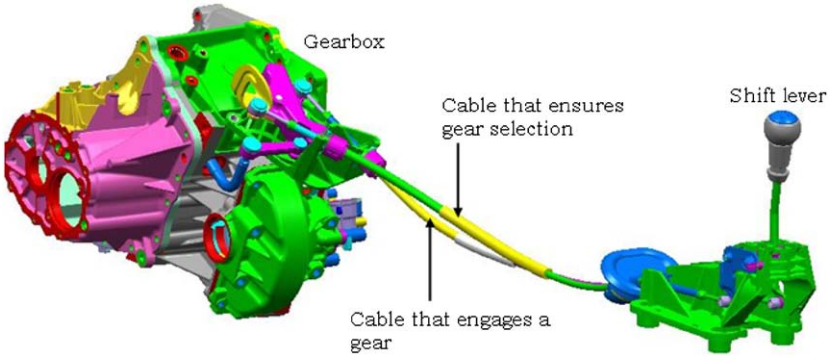

Fig. 1. Setup of a manual gearshift cable in a car.

Fig. 2. Close up of the cable structure.

Repeated impacts are of great interest in science and engineering because of their complex dynamic behavior. Even a simple one degree of freedom impact oscillator can exhibit many different steady-state responses under harmonic excitation. Shaw and Holmes [1] and many after thoroughly explored different mechanical systems and presented the periodic, quasi-periodic solutions, and the various routes to chaos. Now, studies are extended to multidegree of freedom (mdof) vibro-impacting systems such as ground moling machines [2], ultrasonic percussion drill [3], rotor/stator contacts [4–6], delamination in composite beams [7], and beams with stops [8–10].

Considering the complexity of the structure and the numerical difficulties associated with vibro-impact modelling, the goal of this work is to investigate and model the sources of nonlinearities causing cable tizzing. Therefore, our first concern is the inner wire, which presents many similarities with the one presented by Otrin and Boltezar [11]. As in their study, no axial preload is applied to the cable. The second section investigates the nonlinear effect of the interwire friction in the outer housing undergoing different excitation amplitudes on a sine sweep test bench. Both components are modelled with Euler–Bernoulli beams. The first two sections offer estimates of the Young modulus and Rayleigh damping coefficients to be used in the finite element model. In the third section, the dynamic response of the assembled system is presented and the nonlinear vibro-impacting phenomenon associated to tizzing is studied. In the last section, a complete finite element model is proposed in which the inner wire is constrained in its housing with node-to-node gap elements. Finally the computed time series are compared with the experimental measurements.

2. Identification of the inner wire's characteristics

The inner wire is composed of 19 steel wires: one center wire covered by six left laid helical wires, which are again covered by 12 right laid helical wires. This strand is wrapped in an outer helical band. The total diameter is 3.2 mm. Fig. 3(a) illustrates the cross-section of the wire. It has the same characteristics as the cables studied by Otrin and Boltezar [11]. In their work, they considered using Euler–Bernoulli beams to compute the vibration transmissibility of straight and curved cables with no axial preload. An experimental test bench was set up to validate the model and their results proved to be reliable when the elasticity modulus is frequency dependent and the Rayleigh coefficients are dependent of the length of the cable. The Rayleigh damping coefficients α and β define a proportional viscous damping where the damping matrix **C** is

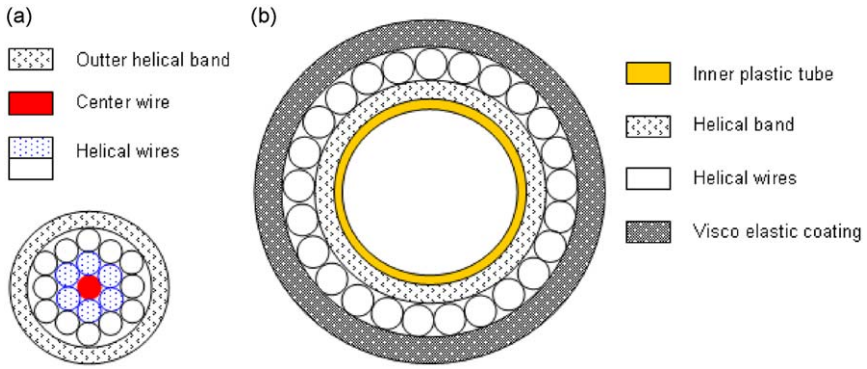

Fig. 3. Cross-sections of the inner wire and the protective housing.

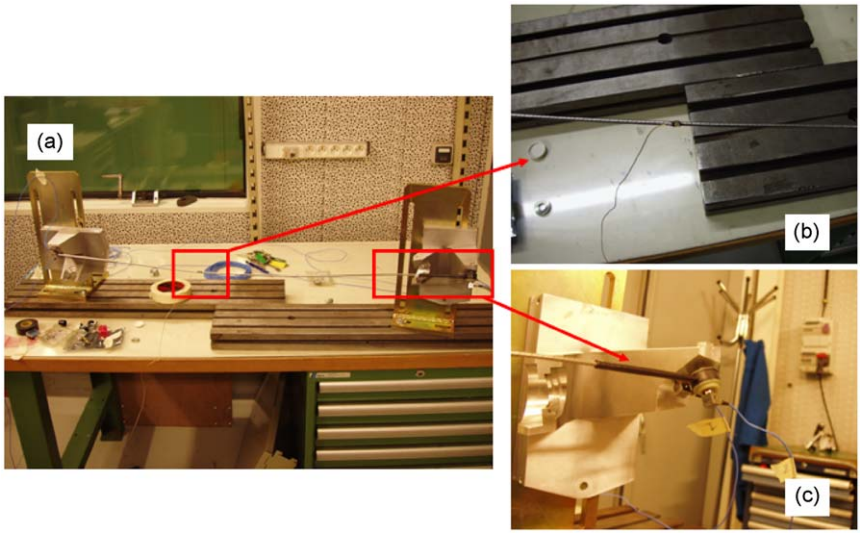

Fig. 4. Experimental setup used for identification of the inner cable: (a) complete setup, (b) accelerometer and (c) cable supports.

related to the mass **M** and stiffness **K** matrix (see [17]) by

$$\mathbf{C} = \alpha\mathbf{M} + \beta\mathbf{K} \tag{1}$$

We present a similar approach to identify the wire's characteristics in the following paragraphs.

2.1. Experimental setup

The length of our cable being different (0.85 m), we could not directly use the results of Otrin and Boltezar's [11] study. We therefore conducted a hammer impact test to determine the eigenfrequencies of the fixed–fixed wire. Fig. 4 presents the experimental setup. The cable abutments used on vehicle were used to obtain the fixed–fixed condition (Fig. 4(c)). Because of the cable's small size, consistent impact on the cable could not be achieved, thus the support was chosen as the impact point. A lightweight accelerometer was glued on the cable to measure the response (Fig. 4(b)). With such an approach, the cable's behavior was determined as if it was fixed to the gearbox.

2.2. Identification

The following identification process in the frequency domain was used to determine a unique homogeneous Young modulus: the first six eigenfrequencies were localized, and a least-square minimization was carried out. The

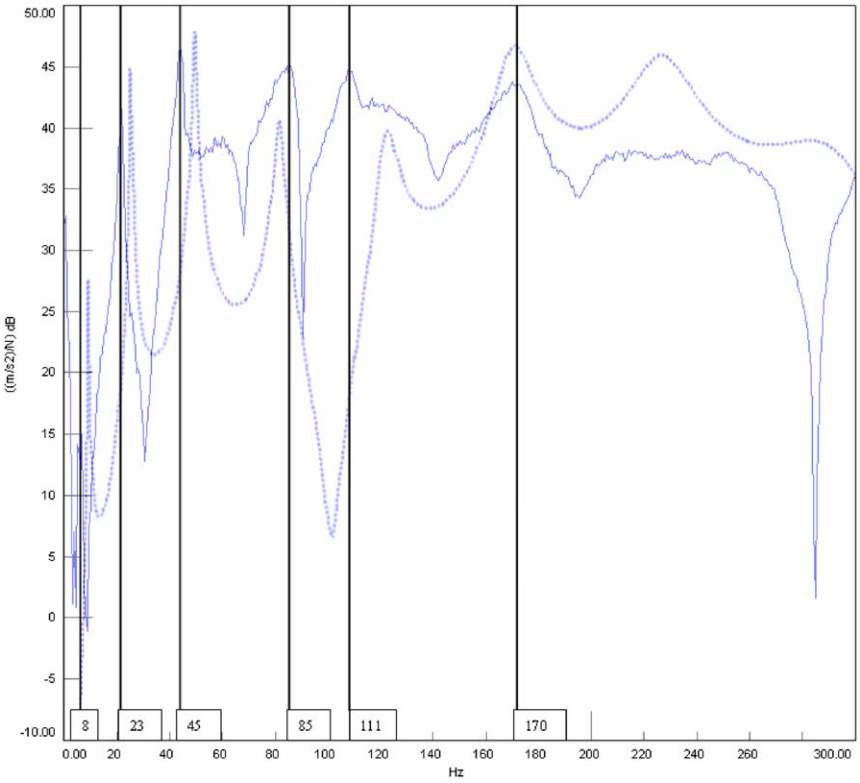

Fig. 5. Comparison of the experimental and computed FRF's of the inner cable (–) measurement (···) computation.

eigenfrequencies were estimated with the theoretical eigenfrequencies of a fixed–fixed Euler–Bernoulli beam

$$f_i = \frac{1}{2\pi}\sqrt{\frac{EI\beta_i^4}{\rho SL^4}} \tag{2}$$

where f_i is the i- th eigenfrequency, E the Young's modulus, I the second area moment, ρ the mass density, S the cross-section and L the length of the beam. β_i is a solution of the well-known transcendental equation

$$1 + \cos(\beta L).\cosh(\beta L) = 0 \tag{3}$$

An iterative procedure was then used to determine the best Rayleigh coefficients to fit the amplitude of the simulated response to the experimental response. The identified Young's modulus is $4 \times 10^{10}\,\mathrm{N\,m^{-1}}$ and the Rayleigh coefficients are $\alpha = 0.8269\,\mathrm{s^{-1}}$ and $\beta = 7 \times 10^{-5}\,\mathrm{s}$. For the sake of simplicity, we did not completely adopt Otrin and Boltezar's [11] approach in which the Young modulus depends on the frequency. Fig. 5 compares the measured and computed frequency response functions of the cable. As seen, the response functions are quite different for several reasons. First of all, the cable abutments are not modelled. Secondly, the fixed–fixed conditions are not totally achieved in the experimental setup and finally, the lighweight accelerometer was not accounted for in the model. However, we will see in Section 5 that these approximations are sufficient to correctly reproduce cable tizzing.

3. Identification of the housing's characteristics

As stated in the introduction, the whole gearshift system is influenced by the motor's fundamental excitations between 20 and 200 Hz. Therefore it is important to estimate the modal parameters of the inner wire and housing in this frequency bandwidth. In the automotive industry, qualification and transmissibility analysis of the gearshift mechanism is usually done in the frequency range of 20–1000 Hz because the dynamics in the gearbox generate excitation frequencies above 200 Hz. Nevertheless, in our case we are interested in cable tizzing, which is independent of the high frequencies generated by the gearbox.

As seen in Fig. 3(b), the housing has a composite structure. A plastic tube is the first layer and is the one in contact with the inner wire. It is then covered by a helical band similar to the one wrapping the inner wire. Extra rigidity is added by a

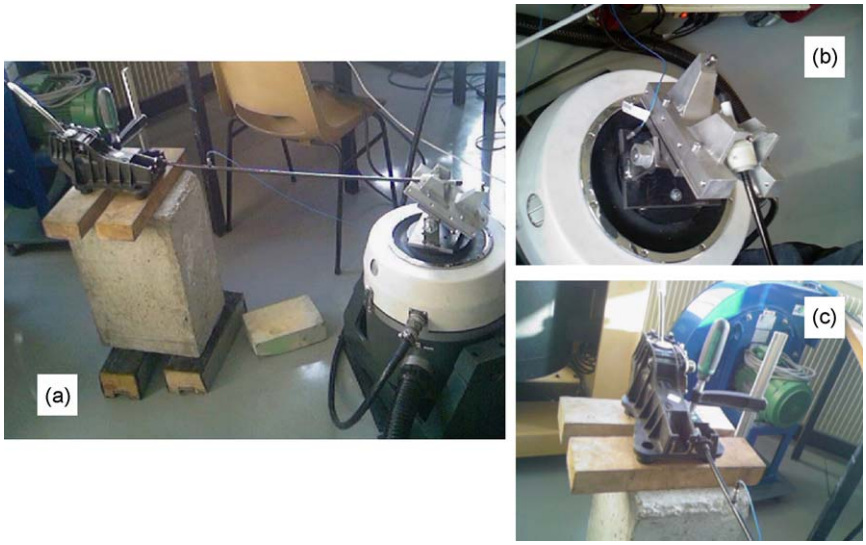

Fig. 6. Experimental setup used to test the outer housing: (a) complete setup, (b) attachment on shaker and (c) attachment on shift box.

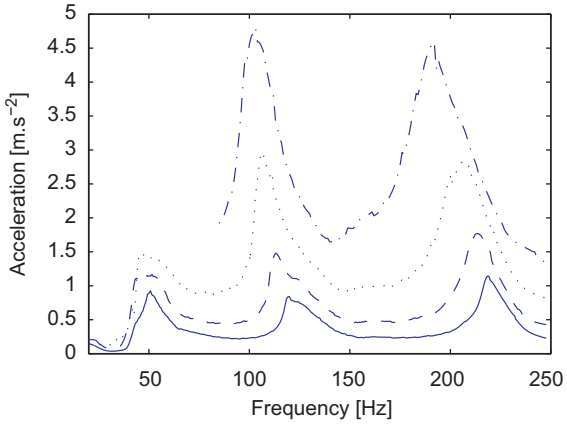

Fig. 7. Measured housing's acceleration output for different excitation amplitudes: (–) 0.5 m s^{-2}, (- -) 1 m s^{-2}, (···) 2 m s^{-2} and (-·-) 4 m s^{-2}.

layer of helical wires and finally a viscoelastic coating is added to protect the cables from wear and high temperatures. It is 0.68 m long.

3.1. Experimental setup

Because of the high damping rates induced by the complex structure of the housing, a hammer test was no longer sufficient. Fig. 6(a) presents the experimental setup. The housing is attached to the shaker by a metallic part that imitates the gearbox attachments (Fig. 6(b)). This piece has no modes below 500 Hz. The other end of the housing is attached to the shift box as it would be in a vehicle (Fig. 6(c)). A slow sine sweep is applied to an electrodynamic shaker and constant input acceleration is controlled by the means of an accelerometer. The housing's acceleration response is measured at 135 mm from the end that is attached to the shift box. Our approach is different from the usual transmissibility analysis where the response is measured in terms of force on the cable's supports. Such a measurement requires modifying the supports, and we did not want influence the global dynamic behavior of the housing with its abutments.

Fig. 7 shows the results of the sine sweeps for different levels of constant input accelerations between 20 and 250 Hz. The amplitude of the first harmonic is presented. Some responses are cutoff because the shaker could not insure the imposed acceleration assignment. As the excitation increases, the eigenfrequencies shift to the left of the spectrum. Such a shift is known in cable structures and is due to interwire friction. As the excitation level rises, the interwire friction is freed and the structure becomes less rigid. Detailed reviews can be found in the works of Elata et al. [12] or Raoff and Davies [13].

Moreover, the distorted aspect of the curves for the lower excitation amplitudes are typical of dry friction systems [14]. However, since the abutments are an assembly of rubber and plastic pieces, the rubber and additional contacts could also contribute to the observed softening.

Generally, Jenkin and Masing elements are used to model the hysteresis present in bending slack cables. Sauter [15] uses this approach to model Stockbridge dampers. But, identifying the parameters that vary along the cable is a cumbersome task. Therefore a simpler approach is used here which is adaptable to large scale problems. It is similar to the ones used by Zhu and Meguid [16] and Otrin and Boltezar [11]. All the nonlinear effects are included in a variable elasticity modulus: for each excitation amplitude the cable will have a different Young's modulus. The Rayleigh damping coefficients will follow a similar rule.

3.2. Identification of the housing's parameters

Once the sine sweep is done, an identification process in the frequency domain is used to determine the Young modulus and Rayleigh damping coefficients for each excitation amplitude. An iterative procedure is used to fit the eigenfrequencies and amplitudes of the simulated response to the experimental response on the third and fourth modes. A finite element Euler–Bernoulli beam is used to compute the simulated response. One end of the beam is fixed to the support, and at the other an acceleration perpendicular to the housing is applied. The equation used to determine the simulated output responses is the following:

$$\mathbf{M}\ddot{\mathbf{U}} + \mathbf{C}\dot{\mathbf{U}} + \mathbf{K}\mathbf{U} = \mathbf{F}_{\text{ext}} e^{i\omega t} \tag{4}$$

where **M**, **C**, **K** are respectively the mass, damping and stiffness matrix. **C** is given by Eq. (1). $\mathbf{F}_{\text{ext}}$ is the amplitude of the imposed harmonic excitation and **U** the displacement. We can directly seek for the stationary solution in the form

$$\mathbf{U}(t) = \tilde{\mathbf{U}} e^{i\omega t + \phi} \tag{5}$$

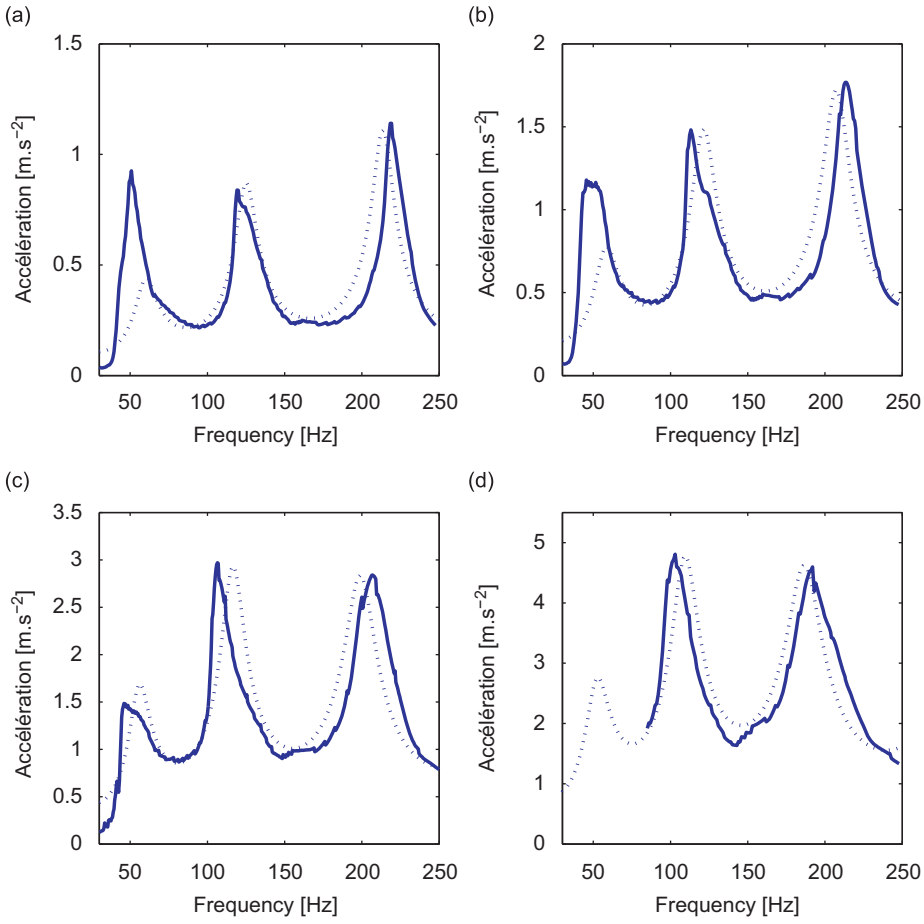

Fig. 8. Comparison of measured (–) and simulated (···) acceleration outputs for different input excitation amplitude: (a) 0.5 m s^{-2}, (b) 1 m s^{-2}, (c) 2 m s^{-2} and (d) 4 m s^{-2}.

where $\tilde{\mathbf{U}}$ corresponds to the harmonic displacements, ω the excitation pulsation and ϕ the phase. Substituting this equation in (4) yields

$$[-\omega^2\mathbf{M} + \mathrm{i}\omega\mathbf{C} + \mathbf{K}] \cdot \tilde{\mathbf{U}} = \mathbf{F}_{\mathrm{ext}} \tag{6}$$

We concentrate here on the third and fourth modes because experience shows that tizzing is more important for the corresponding motor regimes. Fig. 8 compares the measured output responses and the computed responses. As expected, comparison is very good on the third and fourth modes for the different excitation levels, whereas on the second mode correlation is uneven. Table 1 presents the equivalent elasticity modulus and Rayleigh damping coefficients for each excitation amplitude. The modal damping rates ξ_i are determined by the following relationship [17]:

$$\xi_i = \frac{1}{2} \cdot \left(\frac{\alpha}{\omega_i} + \beta\omega_i \right)$$

Table 1
Identified Young modulus and Rayleigh coefficients of the outer housing.

Input level ($\mathrm{m\,s^{-2}}$)	E ($10^{10}\,\mathrm{N\,m^{-1}}$)	α ($\mathrm{s^{-1}}$)	β (10^{-5} s)	ξ_3	ξ_4
0.5	1.419	90	0.05	5.7	3.4
1.0	1.337	97	0.95	6.7	4.3
2.0	1.233	83	3.1	6.8	5.3
4.0	1.087	95	4.0	8.3	6.4

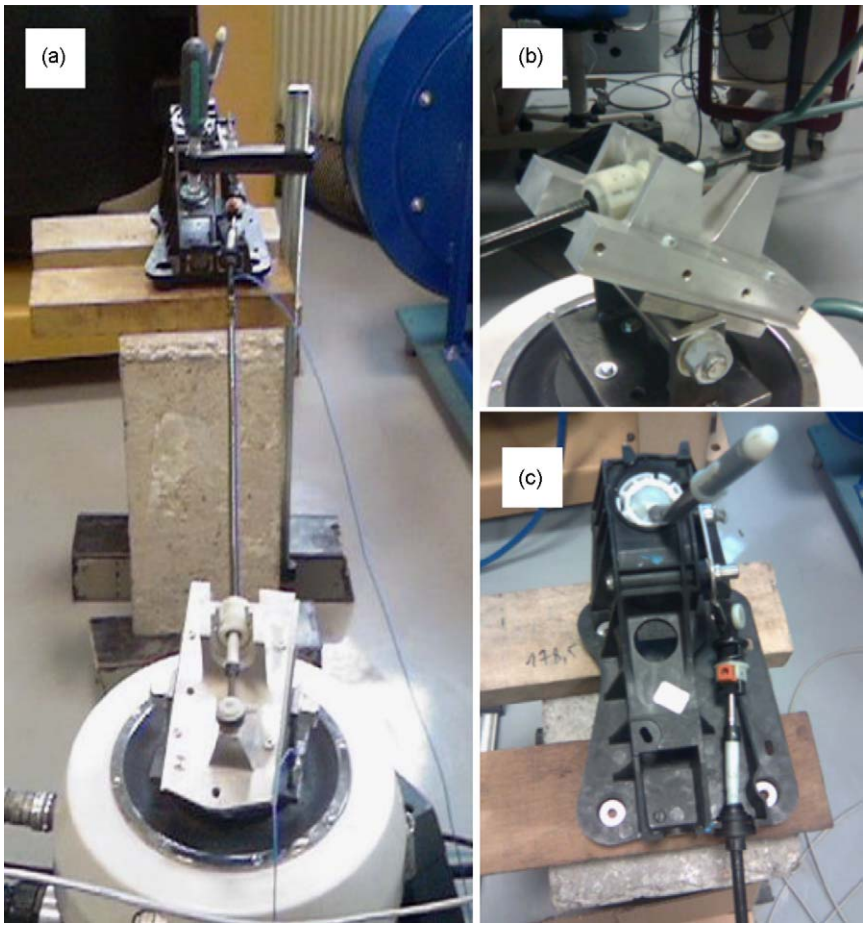

Fig. 9. Experimental setup with inner wire and outer housing: (a) complete setup, (b) attachment on shaker and (c) attachment on shift box.

where ω_i is the i-th eigenfrequency, and α and β are the Rayleigh coefficients defined by Eq. (1). As seen, the critical damping rates for modes 3 and 4 are relatively high and increase with the input level. Much higher values have previously been encountered in the literature for simple slack cable structures [16].

In the two previous sections simplified models were proposed and identified to represent the dynamic behavior of complex cable structures. Since the strains and displacements are small, a linear beam theory was used and proportional Rayleigh coefficients reproduced the global damping of the cables. However, for different excitation amplitudes different elasticity modulus and damping coefficients were estimated to account for the nonlinear effects in the outer housing. Such an approach is motivated by the need to have a simple model transposable to large scale engineering problems.

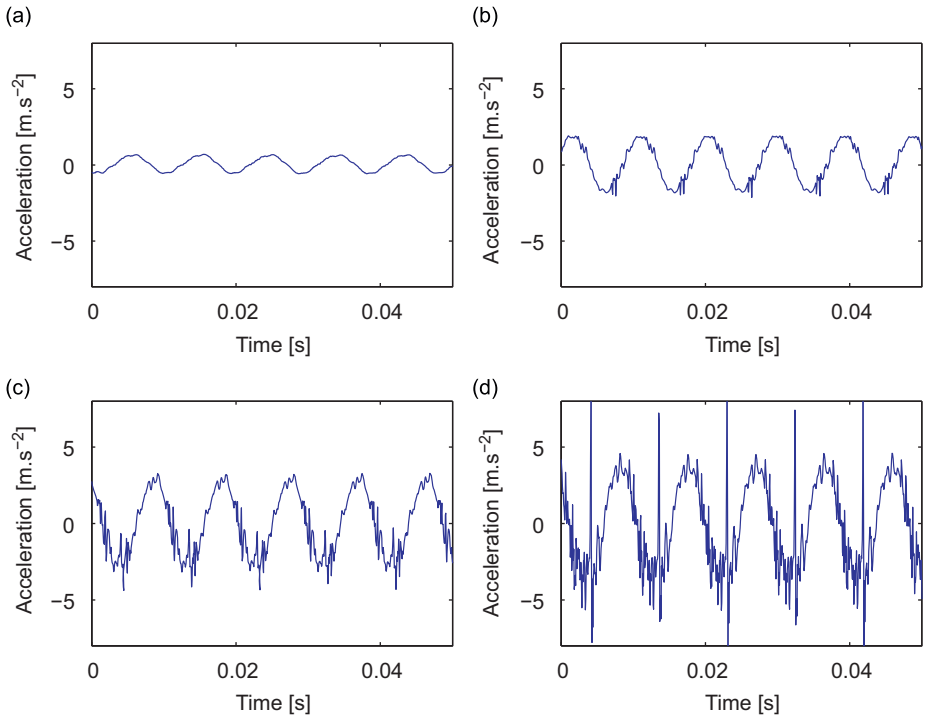

Fig. 10. Measured time responses at 106 Hz for different excitation amplitudes: (a) 0.5 m s^{-2}, (b) 1 m s^{-2}, (c) 2 m s^{-2} and (d) 4 m s^{-2}.

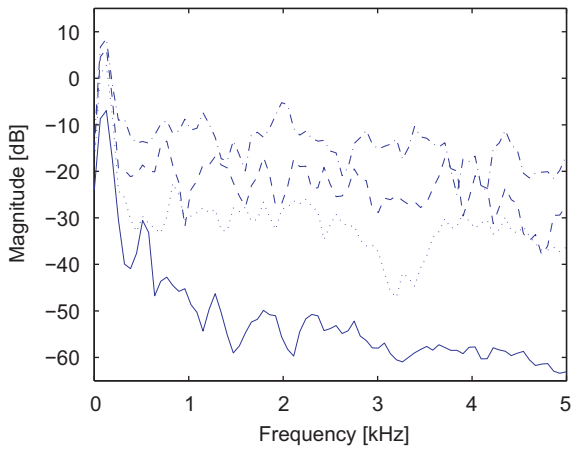

Fig. 11. Magnitude spectrums of time series for an excitation of 106 Hz for different levels: (–) 0.5 m s^{-2}, (···) 1 m s^{-2}, (--) 2 m s^{-2} and (- ·) 4 m s^{-2}.

4. Output response of the assembled inner wire and housing

4.1. Experimental setup

In this section we present the experimental results of the shaker tests applied to the assembled system. Fig. 9(a) presents the experimental setup. The inner wire is set inside its housing and both pieces are linked to the shaker in the same way they would be attached in a vehicle (Fig. 9(b)). The other end is attached to the shift box (Fig. 9(c)). The whole system undergoes the shaker's excitation. Time series were measured to determine the steady-state dynamic behavior of the gearshift cable for different forcing frequencies and amplitudes.

4.2. Experimental results

Fig. 10 shows the measured time series for an excitation frequency of a 106 Hz. For the lowest input level (Fig. 10(a)) the response is a sine function of the same frequency as the excitation. In this case there is no tizzing. As input acceleration increases (Figs. 10(b)–(d)) a periodic high frequency signal is superimposed to the base sine signal. Cable tizzing is the source of this high frequency signal. Physically, it corresponds to periodic impacts between the inner wire and its housing. Fig. 11 compares the magnitude spectrums of each time signal. As the excitation level increases, the high frequency content also increases. A similar behavior can be noticed at 186 Hz (Fig. 12). Impacts between cable and housing appear at 1 m s^{-2} (Fig. 12(b)) and increase with the excitation level. Another interesting phenomenon is worth pointing out: for an excitation amplitude of 4 m s^{-2} (Fig. 12(d)) the response signal has a period twice as long as the forcing period. This kind of behavior occurs in nonlinear systems after a period-doubling bifurcation and is well documented in Nayfeh and Balachandran [18].

5. The complete finite element model

In the previous sections were presented the vibro-impacting phenomenon and the model parameters that can be used to represent the dynamic behavior of the inner wire and its housing. Considering the difficulty of modelling multiple impact systems, we chose the simplest finite element model that could represent the behavior of the assembled gearshift cable. The inner wire is considered to be linear and we use the previously identified homogeneous Young's modulus and Rayleigh coefficients. The inner wire is 0.73 m long and its supports are not modelled, even though their effects on the behavior are included in the identified parameters. The protective housing has a nonlinear behavior depending on the excitation amplitude. It is 0.68 m long.

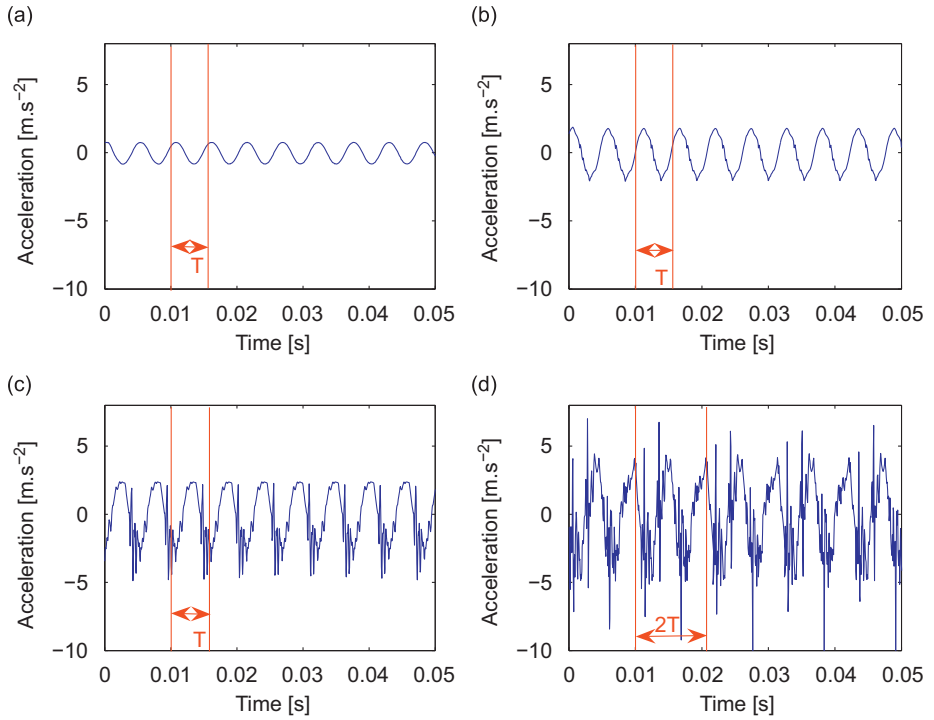

Fig. 12. Measured time responses at 186 Hz for different excitation amplitudes: (a) 0.5 m s^{-2}, (b) 1 m s^{-2}, (c) 2 m s^{-2} and (d) 4 m s^{-2}.

The inner wire is composed of 73 Euler–Bernoulli beam elements, and the housing of 68 Euler–Bernoulli beam elements. To constrain the wire in its protective housing 31 node-to-node gap elements are added. The gap at each node is set at 0.25 mm. At the shift box side, the inner wire and housing have fixed boundary conditions. At the gearbox side, the boundary conditions are free. Harmonic excitation was applied to the vertical degree-of-freedom of the wire and housing at the gearbox end. After a static step, during which gravity was applied to both components, the steady-state response was computed using a modified Newmark's integration scheme. Application of the gravity was necessary to initialize the contacts between the inner wire and housing. The contact law was considered to be plastic and when contact occurred, the constraint was enforced with Lagrange multipliers. More details on the used algorithm can be found in Abaqus [19]. The complete finite element model after the first static step is presented in Fig. 13.

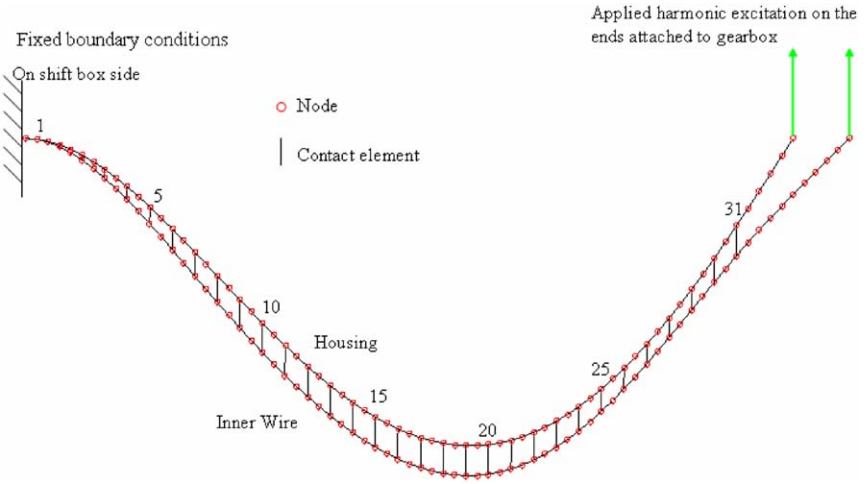

Fig. 13. Complete finite element model after the first static step.

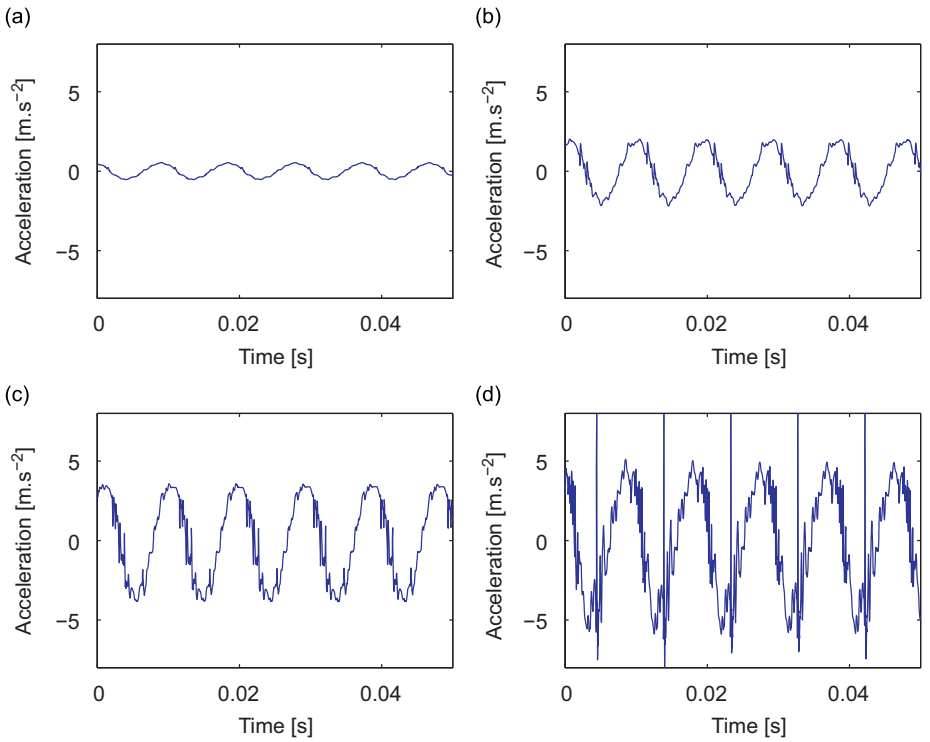

Fig. 14. Computed time series at 106 Hz for different excitation amplitudes: (a) 0.5 m s^{-2}, (b) 1 m s^{-2}, (c) 2 m s^{-2} and (d) 4 m s^{-2}.

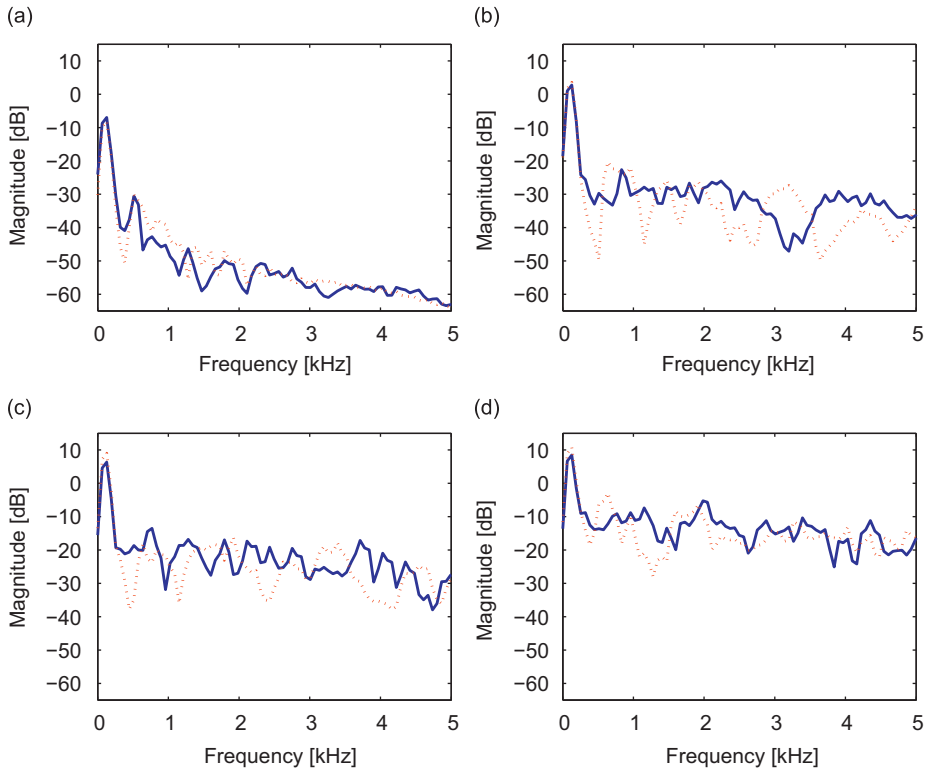

Fig. 15. Comparison of measured (–) an computed (···) magnitude spectrums for 106 Hz and different excitation amplitudes: (a) 0.5 m s^{-2}, (b) 1 m s^{-2}, (c) 2 m s^{-2} and (d) 4 m s^{-2}.

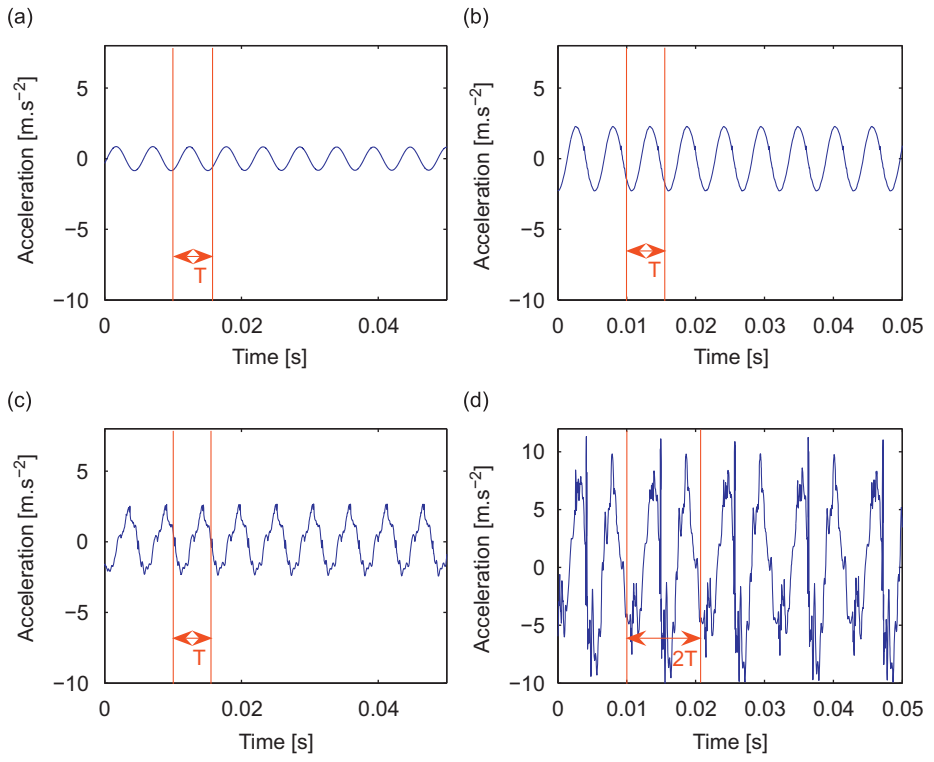

Fig. 16. Computed time series at 186 Hz for different excitation amplitudes: (a) 0.5 m s^{-2}, (b) 1 m s^{-2}, (c) 2 m s^{-2} and (d) 4 m s^{-2}.

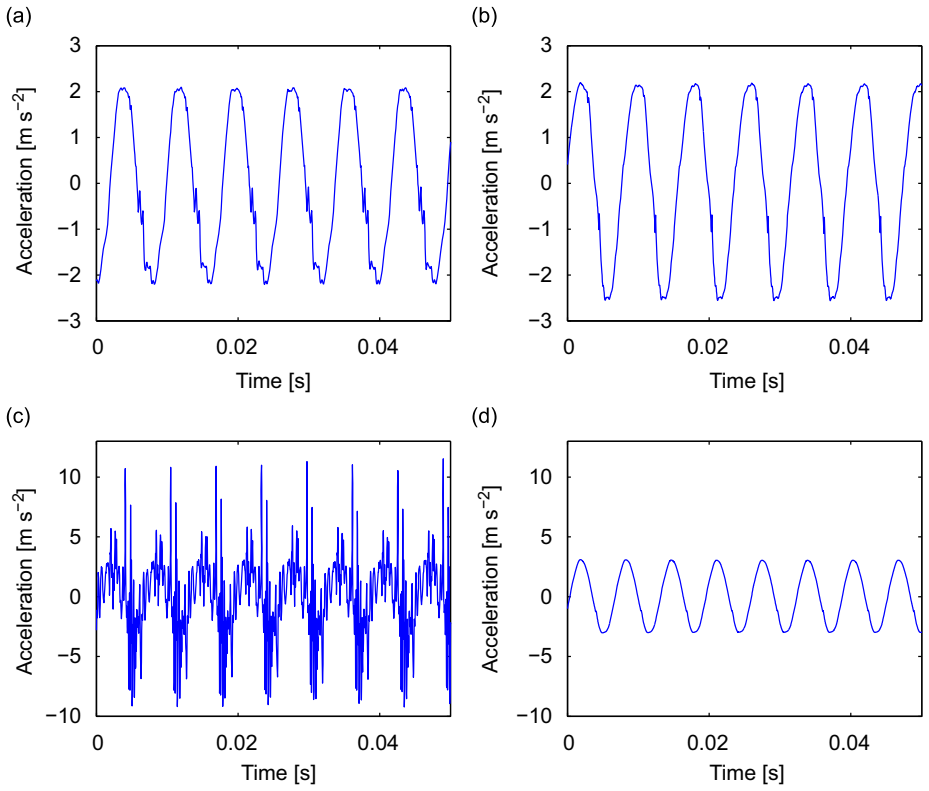

Fig. 17. Comparison of measured (a, c) and computed (b, d) time series for an input level of 4 m s^{-2} at 126 Hz (a, b) and 156 Hz (c, d).

5.1. Computation results

Fig. 14 presents the computed time series for different excitation amplitudes at 106 Hz. Correlation with the measured acceleration responses is very good and the model exhibits the same behavior as the real gearshift cable for all excitation amplitudes. Cable tizzing appears for an excitation of 1 m s^{-2} (Fig. 14(b)) and the impacts occur at the same phase as on the measured data. Fig. 15 compares the magnitude spectrums of the measured and computed time series for 106 Hz. For all excitation levels, the high frequency content is similar.

Fig. 16 presents the computed time series for 186 Hz. Even if the overall levels are not as accurate as for 106 Hz, the dynamic behavior is well represented and tizzing appears at 2 m s^{-2} (Fig. 16(c)). For an input acceleration of 4 m s^{-2}, a period doubled response is also computed (Fig. 16(d)).

Figs. 17(a) and (b) compare the measured and computed response for an excitation level of 4 m s^{-2} and frequency of 126 Hz. Once again the computation offers good correlation with the measurements. No high frequencies are observed in the time series, as there is no interaction between the inner wire and its housing. Figs. 17(c) and (d) compare the measured and computed response for the same excitation level at a frequency of 156 Hz. This time both time series are not comparable. For this excitation frequency there is a localized mode in which the inner wire's and housing's abutments interact strongly. Since these parts are not explicitly included in the model we cannot expect to reproduce their effect.

6. Conclusions

In this paper, we investigated cable tizzing. It is a vibro-impact phenomenon found in gearshift cables: for certain excitation frequencies and amplitudes an annoying tizzing sound is heard. We showed here that it actually consists of multiple impacts between the inner wire and the protective housing when undergoing the motor's vibrations. Because the inner wire and housing both have complex cable structures, it was necessary to find simple models that could be used efficiently in time stepping algorithms. Therefore a linear beam theory was used to model the inner wire. Its homogeneous Young's modulus and unique Rayleigh coefficients were determined with a hammer test. The linear beam theory was also used for the housing. However, because of the nonlinear effects due to the interwire friction, the abutments and boundary conditions, variable elasticity modulus and Rayleigh damping coefficients were used. They are dependent on the excitation level and were determined with a swept sine test. Once models for the inner wire and for the housing were established,

they were assembled in the final finite element model in which the inner wire is constrained in the housing with gap elements. The numerical computations yield results that are comparable with the experimental measurements: tizzing appears at the same frequencies and excitation amplitudes, even dynamic instabilities are predicted by the model.

Keeping in mind these encouraging results, we must not forget several shortcomings of the model. First of all, cable tizzing is sensitive to the modes of the inner wire and the housing. Therefore the modes at each frequency must be correctly determined. In this paper, the elastic modulus of the housing depends on the excitation amplitude but for a better correlation it should also be a function of the excitation frequency. A better identification of the inner wire could also help improve the correlation results for all excitation frequencies. Secondly, the inner wire's and housing's abutments have not been modelled. As we have seen, for certain excitation frequencies (156 Hz) their influence can be important. Finally, it would be interesting to carry out a full parametric study to determine the influence of the different parameters on the response of the system. Our future work will be oriented in these directions.

References

[1] S.W. Shaw, P. Holmes, A periodically forced piecewise linear oscillator, *Journal of Sound and Vibration* 90 (1) (1983) 129–155.
[2] K.C. Woo, A.A. Rodger, R.D. Neilson, M. Wiercigroch, Application of the harmonic balance method to ground moling machines operating in periodic regimes, *Chaos, Solitons, and Fractals* 11 (2000) 2515–2525.
[3] C. Potthast, J. Twiefel, J. Wallascek, Modelling approaches for an ultrasonic percussion drill, *Journal of Sound and Vibration* 308 (2007) 405–417.
[4] G. Von Groll, D.J. Ewins, The harmonic balance method with arc-length continuation in rotor/stator contact problems, *Journal of Sound and Vibration* 241 (2) (2001) 223–233.
[5] M. Azeez, A.F. Vakakis, Numerical and experimental analysis of a continuous overhung rotor undergoing vibro-impacts, *International Journal of Nonlinear Mechanics* 34 (1999) 415–435.
[6] N. Lesaffre, J.J. Sinou, F. Thouverez, Stability analysis of rotating beams rubbing on an elastic circular structure, *Journal of Sound and Vibration* 299 (2007) 1005–1032.
[7] P. Vielsack, A vibro-impact model for the detection of delamination, *Journal of Sound and Vibration* 253 (2) (2002) 347–358.
[8] M. Trindade, C. Wolter, R. Sampaio, Karhunen-loève decomposition of coupled axial/bending vibrations of beams subject to impacts, *Journal of Sound and Vibration* 279 (2005) 1015–1036.
[9] J. Knudsen, A.R. Massih, Impact oscillations and wear of loosely supported rod subjected to harmonic load, *Journal of Sound and Vibration* 278 (2004) 1025–1050.
[10] D. Wagg, S.R. Bishop, Application of non-smooth modelling techniques to the dynamics of a flexible impacting beam, *Journal of Sound and Vibration* 256 (5) (2002) 803–820.
[11] M. Otrin, M. Boltezar, Damped lateral vibrations of straight and curved cables with no axial preload, *Journal of Sound and Vibration* 300 (2007) 676–694.
[12] D. Elata, R. Eshkenazy, M.P. Weiss, The mechanical behavior of a wire rope with an independent wire rope core, *International Journal of Solids and Structures* 41 (5–6) (2004) 1157–1172.
[13] M. Raoff, T.J. Davies, Simple determination of the maximum axial and torsional energy dissipation in large diameter spiral strands, *Computers and Structures* 84 (2006) 676–689.
[14] S. Nacivet, C. Pierre, F. Thouverez, L. Jezequel, A dynamic Lagrangian frequency time method for the vibration of dry friction damped systems, *Journal of Sound and Vibration* 265 (2003) 201–219.
[15] D. Sauter, Modelling the Dynamic Characteristics of Slack Wire Cables in Stockbridge Dampers, Dr. Ing. Dissertation, Department of Applied Mechanics, Darmstadt University of Technology, Germany, 2003.
[16] Z.H. Zhu, S.A. Meguid, Nonlinear FE-based investigation for flexural damping of slacking wire cables, *International Journal of Solids and Structures* 44 (2007) 5122–5132.
[17] K.J. Bathe, *Finite Element Procedures in Engineering Analysis*, Prentice-Hall, Englewoods Cliffs, NJ, 1982.
[18] A. Nayfeh, B. Balachandran, *Applied Nonlinear Dynamics: Analytical, Computational, and Experimental Methods*, Wiley, New York, 1995.
[19] Abaqus documentation Theory Manual V6.7, section 2.4.2, Intermittent contact/impact.